A&A 463, 513–518 (2007)
DOI: 10.1051/0004-6361:20066386


Astronomy & Astrophysics

# Simulations of metal enrichment in galaxy clusters by AGN outflows

R. Moll[1], S. Schindler[1], W. Domainko[1,3], W. Kapferer[1], M. Mair[1], E. van Kampen[1], T. Kronberger[1], S. Kimeswenger[1], and M. Ruffert[2]

[1] Institut für Astro- und Teilchenphysik, Universität Innsbruck, Technikerstraße 25, 6020 Innsbruck, Austria
e-mail: rmo@mpa-garching.mpg.de
[2] School of Mathematics, University of Edinburgh, Edinburgh EH9 3JZ, Scotland, UK
[3] Max-Planck-Institut für Kernphysik, Saupfercheckweg 1, 69117 Heidelberg, Germany

Received 12 September 2006 / Accepted 17 October 2006

**ABSTRACT**

*Aims.* We assess the importance of AGN outflows with respect to the metal enrichment of the intracluster medium (ICM) in galaxy clusters.
*Methods.* We use combined $N$-body and hydrodynamic simulations, along with a semi-numerical galaxy formation and evolution model. Using assumptions based on observations, we attribute outflows of metal-rich gas initiated by AGN activity to a certain fraction of our model galaxies. The gas is added to the model ICM, where the evolution of the metallicity distribution is calculated by the hydrodynamic simulations. For the parameters describing the AGN content of clusters and their outflow properties, we use the most observationally favorable values.
*Results.* We find that AGNs have the potential to contribute significantly to the metal content of the ICM or even explain the complete abundance, which is typically $\sim 0.5\ Z_\odot$ in core regions. Furthermore, the metals end up being inhomogeneously distributed, in accordance with observations.

**Key words.** galaxies: clusters: general – galaxies: active – X-rays: galaxies: clusters – galaxies: quasars: absorption lines – galaxies: jets

## 1. Introduction

### 1.1. The ICM and its composition

The main baryonic component of galaxy clusters is the intracluster medium (ICM), a hot ($10^{7...8}$ K), X-ray emitting plasma. Observations made with modern X-ray observatories like Chandra (e.g. Vikhlinin et al. 2005) or XMM Newton (e.g. Tamura et al. 2004) have revealed that the chemical composition of the ICM is clearly non-primordial, with metal abundances on the order of $\sim 0.5\ Z_\odot$. Furthermore, metallicity maps are available for the core regions of some very bright clusters (e.g. Sanders et al. 2004; Hayakawa et al. 2004; Durret et al. 2005). Apart from confirming the occurrence of high abundances, these also reveal that the metals are distributed inhomogeneously.

Since heavy elements can only be produced by means of stellar or explosive nucleosynthesis, it is obvious that they originate mainly in cluster-member galaxies. This requires transfer processes that remove the metals from the galaxies. Among the first transfer processes to be suggested were ram-pressure stripping of interstellar gas (Gunn & Gott 1972) and galactic winds (De Young 1978).

Various groups have performed simulations of metal enrichment in clusters. De Lucia et al. (2004) used a combination of $N$-body simulations and semi-analytic techniques to follow the formation, evolution, and chemical enrichment of galaxies, including flows of gas and metals into and out of galaxies. They find that most of the metals currently in the ICM have been ejected at $z > 1$ and that massive galaxies are the largest contributors to the ICM metallicity. Nagashima et al. (2005) took a similar approach with similar results. However, both groups do not predict the distribution of the metals in a cluster. Tornatore et al. (2004) combined $N$-body and SPH (smoothed particle hydrodynamics) simulations to create metallicity profiles for clusters, with a model that includes star formation, as well as supernovae to produce heavy elements, but did not distinguish between different metal transport processes.

The simulations of our group distinguish not only between different metal transfer processes, but also between the ICM and the gas that belongs to galaxies. The enrichment efficiency of ram-pressure stripping, galactic winds, and merger-driven starbursts have been studied by Domainko et al. (2006), Kapferer et al. (2006), and Schindler et al. (2005). Both processes were found to be able to significantly enrich the ICM, but they are not sufficient enough to explain the complete abundance. Galaxy-galaxy interactions and intracluster supernovae (Kapferer et al. 2005; Domainko et al. 2004) have also been found to be possible contributors to the metal content of the ICM.

In this paper, we demonstrate that AGNs can also contribute significantly to the metallicity of the ICM. So far, investigations of the impact of AGNs on galaxy clusters have been oriented almost exclusively towards the heating of the ICM (e.g. Sijacki & Springel 2006), as this provides a possible solution to the cooling flow problem. In this work, however, we do not put the emphasis on energy transfer, but on metal transfer.

### 1.2. AGNs and outflows

Observational evidence of wind-like outflows from AGNs exists in the form of blueshifted absorption lines in UV and X-ray spectra. These lines are supposed to be created by matter moving away from the AGN, often with very high velocities on the order of thousands of $\mathrm{km\,s^{-1}}$ or even relativistic speeds (e.g. Chartas et al. 2003). Reviews of the subject can be found in Crenshaw et al. (2003) and Veilleux et al. (2005). The absorption occurs at various distances from an AGN's central engine, from the subkiloparsec to a galactic scale, and in both radio-quiet and radio-loud AGNs. The inferred mass outflow rates are vague: Crenshaw et al. (2003) conclude that they are comparable to the mass accretion rates (which would likely leave a wide range from $\lesssim 0.001\ M_\odot\ \mathrm{yr}^{-1}$ for low-luminosity AGNs to $\sim 100\ M_\odot\ \mathrm{yr}^{-1}$ for quasars and powerful radio galaxies), and Veilleux et al. (2005) propose the range $0.1 \ldots 10\ M_\odot\ \mathrm{yr}^{-1}$ and suggest that there is a strong mass-loading of the outflow by the galactic ISM. Morganti et al. (2005) assessed outflow rates ranging from $\sim 1$ to over $50\ M_\odot\ \mathrm{yr}^{-1}$ from the spectra of several radio-loud AGNs and estimated that the kinetic energy of the outflows might be sufficient to remove the gas from the bulges of the galaxies. A very distant ($r \sim 28$ kpc), massive ($\sim 2 \times 10^9\ M_\odot$) absorber was found by Hamann et al. (2001) in the vicinity of a radio-loud AGN, which indicates a mass outflow rate of $\sim 10\ M_\odot\ \mathrm{yr}^{-1}$ provided that the material originates in the AGN and was continuously expelled over an assumed lifetime of $10^8$ yr. The composition of the outflows is likely to be rich in metals: Hamann (1997) gives a lower limit of $\sim Z_\odot$ and says there is evidence of metallicities greater than $10\ Z_\odot$. The possibility of super-solar ICM metallicities around AGNs has been confirmed by the observations of Iwasawa et al. (2001).

The physical origin of these outflows is unclear (Crenshaw et al. 2003; Krolik 1999). Speculations include winds driven by heat, radiation pressure, and magnetocentrifugal processes. Elvis (2000) proposes an empirically derived, unifying geometrical model for the inner regions of AGNs. It was assembled so as to explain all the absorption and emission features found in AGNs and their occurrence pattern. In this model, the absorption is ascribed to a warm ($\sim 10^6$ K) and highly ionized medium, the "WHIM", which arises vertically from a narrow range of radii on the accretion disk in a funnel-shaped outflow. A self-consistent model that provides ready-to-use outflow properties does not exist yet, however.

AGN jets in clusters are found to be very extended, reaching $\sim 100$ kpc into the ICM (e.g. Owen et al. 1985). Thus, they are an obvious candidate for the transfer of metal-rich matter into the ICM. Morganti et al. (2005), for example, ascribe their findings to interactions between radio jets and the surrounding material. The possibility that AGN entrainment is efficient was confirmed in early simulations of super-sonic jets by De Young (1986), who estimated that a total of $10^{7\ldots9}\ M_\odot$ of ambient material can be entrained by typical jets. This is interesting because an AGN must plough its way through metal-rich regions like the broad emission-line region. The metallicity is probably very high there (Hasinger et al. 2002). Baldwin et al. (2003) found $\sim 15\ Z_\odot$ for the BEL region in one particular quasar. The jets themselves, being outflows per se, are uninteresting with respect to metal enrichment, as they probably consist either of protons and electrons or of electrons and positrons (Hirotani 2005).

Further evidence for galactic mass loss through AGNs is found in semi-analytic models imposed on large-scale structure formation simulations: Croton et al. (2006) find that AGNs are able to alter their host galaxies, thus inducing outflows of gas.

## 2. Methods

In the following subsection, we describe the elementary parts of our galaxy cluster simulations, see Kapferer et al. (2005) for more information. Then, in Sect. 2.2, we explain in detail how AGN outflows were implemented in this framework.

### 2.1. Numerical methods

We use combined $N$-body and hydrodynamic techniques, together with a semi-numerical galaxy-formation code, to simulate the different components of galaxy clusters. The dark-matter $N$-body simulations, which yield the gravitational potential of the dark matter, are performed using a tree code (Barnes & Hut 1986) with constraint realizations of Gaussian random fields as initial conditions (Hoffman & Ribak 1991; van de Weygaert & Bertschinger 1996). The semi-numerical galaxy-formation and evolution code (van Kampen et al. 1999) determines where galaxies form and provides galaxy properties. Finally, the hydrodynamic code models the ICM. It uses the PPM (piecewise parabolic method) with a shock-capturing scheme (Colella & Woodward 1984; Fryxell et al. 1989) and computes the properties of the ICM in four nested, cubical grids (Ruffert 1992), each of which is centered at the cluster center, with the largest having a volume of $(20\ \mathrm{Mpc})^3$ and the smallest $(2.5\ \mathrm{Mpc})^3$. Each grid consists of $128 \times 128 \times 128$ cells. Thus, we obtain the highest resolution in the cluster center. As initial condition for the gas, hydrostatic equilibrium is used. While the $N$-body tree code and the semi-numerical galaxy formation code start at $z = 20$, the hydrodynamic simulation starts at $z = 1$, thus covering only about 58% of the simulation time. We adopt a $\Lambda$CDM cosmology with $\Omega_\Lambda = 0.73$, $\Omega_\mathrm{m} = 0.27$, $\sigma_8 = 0.93$, and $h = 0.7$.

### 2.2. AGN outflows

In the hydrodynamic simulations, outflows from AGNs are added to the model ICM at the respective position of the AGN host galaxy, altering the density, chemical composition, momentum, and energy of the ICM there. An outflow is either put into the cell where the AGN host resides (one cell in the innermost grid has a volume of $(19.5\ \mathrm{kpc})^3$), or it is distributed "jet-like" along a series of cells in the shape of bipolar outflows, emanating from the launching AGN host up to 100 kpc to either side.

To determine the AGN content and characterize the outflows, a series of parameters has been introduced. In the absence of a comprehensive theoretical understanding of AGN triggering and outflows, we have constrained these parameters using values from observations. The AGN fraction $f_\mathrm{AGN}$ is the fraction of galaxies that host AGNs with outflows. Multi-wavelength observations of clusters by Martini et al. (2006) have shown that the value for AGNs in general is about 5%. Assuming that 10% of all AGNs are radio-loud, we obtain $f_\mathrm{AGN} = 0.05$ for outflows attributed to all AGNs (AGN winds) and $f_\mathrm{AGN} = 0.005$ for outflows that are specific to radio-loud AGNs (entrainment by jets). We assume $f_\mathrm{AGN}$ to be fixed with time. Furthermore, we select AGN hosts randomly among the cluster members, relying upon the findings of Miller & Owen (2002), who discovered that the radial distribution of AGNs is similar to that of cluster galaxies in general.

The duty cycle or lifetime $\tau_\mathrm{AGN}$ determines how long an outflow lasts. Martini (2004) finds, collecting a broad variety of estimates, that the lifetime of AGNs is in the range $10^{6\ldots8}$ yr. He also notes that it is not clear whether the activity is episodic, with individual active periods much shorter than the total active

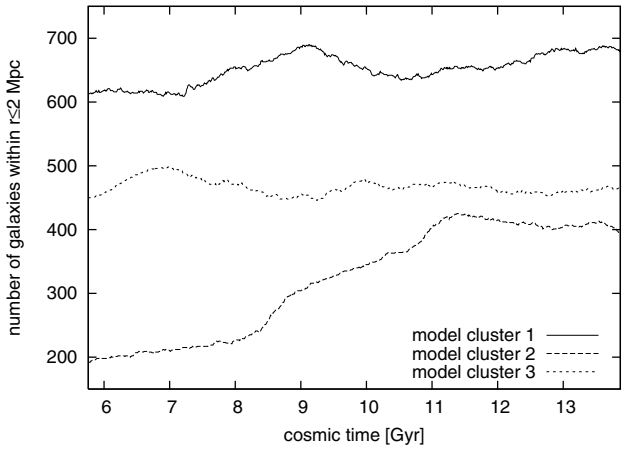


**Fig. 1.** Number of galaxies within $r \leq 2$ Mpc with respect to the cluster center as a function of cosmic time.

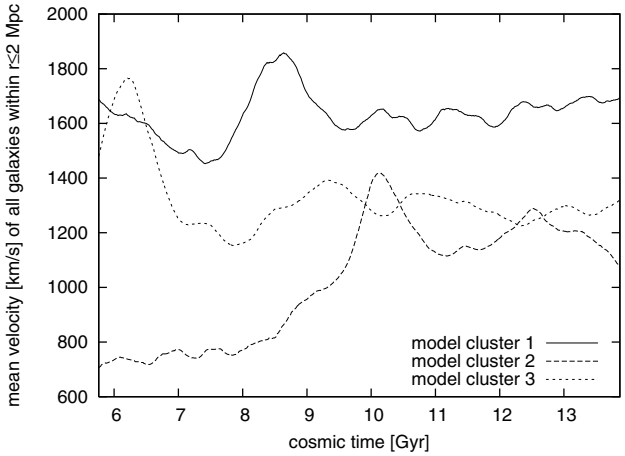


**Fig. 2.** Average absolute value of the velocity of all galaxies within $r \leq 2$ Mpc as a function of cosmic time. The humps indicate merging events.

lifetime. Whether outflows are present during the entire time is also arguable, of course. Nevertheless, we use the upper limit, $\tau_{\rm AGN} = 0.1$ Gyr, as a standard value and refer to Sect. 4.2 for a discussion of the effect of shorter duty cycles.

The mass outflow rate $\dot{M}_{\rm out}$ refers to the amount of material that an AGN galaxy loses to the ICM. As mentioned in Sect. 1.2, there are no good constraints on this quantity from observations, but outflows on the order of solar masses per year seem to be possible in at least some cases. The same holds true for the outflow metallicity $Z_{\rm out}$; the value seems to at least be super-solar (Iwasawa et al. 2001). We adopt 5 $Z_\odot$ as a standard value. Note that the results for different metallicities are easily found, see Sect. 4.2 for details.

Finally, there is the outflow temperature $T_{\rm out}$. We adopt the temperature of the WHIM (warm and highly ionized medium) outflow (see Sect. 1.2) proposed by Elvis (2000), which is $10^6$ K.

## 3. Properties of the model clusters

Three different model clusters have been used in this work. Model cluster 1 is a rich cluster with an extraordinarily deep potential. Galaxies, detached or in small lumps, are attracted by its potential during the time interval in which the ICM is simulated. This and the formation of new galaxies raise the total number of galaxies within $r \leq 2$ Mpc from 613 at $z = 1$ to 679 at $z = 0$, see Fig. 1. This cluster also exhibits the highest average velocities and the highest velocity dispersion, see Table 1.

Model cluster 2 differs considerably from model cluster 1. It contains far fewer galaxies and is characterized by several merging events, which are visible as humps in the average velocity evolution curve shown in Fig. 2. At $z = 1$, the cluster consists mainly of two subclusters, separated by a distance of about 3 Mpc from each other. The subclusters approach each other and start to merge about 4.4 Gyr later. At $z = 0$, the galaxies settle down and form a single cluster with a total of 396 galaxies within $r \leq 2$ Mpc.

Model cluster 3 resembles model cluster 1 but contains fewer galaxies. Because of its size and merging behavior, it can be considered as a standard galaxy cluster. The total number of galaxies within $r \leq 2$ Mpc rises from 449 at $z = 1$ to 464 at $z = 0$, albeit not monotonically. This means that the present size of this cluster, as measured by the galaxy content, lies between clusters 1 and 2. The same holds true for the average galaxy velocity and the velocity dispersion.

**Table 1.** Number of galaxies, average absolute value of the velocity, and velocity dispersion (measured by the population standard deviation) of the three model clusters at $z = 0$, taking only galaxies within $r \leq 2$ Mpc into account.

| Cluster | Number of galaxies | Average velocity [km s$^{-1}$] | Velocity dispersion [km s$^{-1}$] |
|---|---|---|---|
| 1 | 679 | 1694 | 828 |
| 2 | 396 | 1078 | 539 |
| 3 | 464 | 1322 | 623 |

**Table 2.** Average[a] galaxy number density $n$, ICM density $\rho$ and "gas mass per galaxy" $\rho/n$ in runs without AGN outflows, where the super- and subscripts give the greatest fluctuations from the mean.

| Cluster | $n$ [Mpc$^{-3}$] | $\rho$ [$10^{-26}$ kg m$^{-3}$] | $\frac{\rho}{n}$ [$10^{10}$ $M_\odot$] |
|---|---|---|---|
| 1 | $96.6^{+16.8}_{-16.1}$ | $22.2^{+2.4}_{-2.2}$ | $3.4^{+0.4}_{-0.4}$ |
| 2 | $45.1^{+26.2}_{-20.5}$ | $3.1^{+1.0}_{-0.9}$ | $1.1^{+0.5}_{-0.2}$ |
| 3 | $78.4^{+16.6}_{-9.4}$ | $9.6^{+1.1}_{-1.1}$ | $1.8^{+0.1}_{-0.2}$ |

[a] Taken over space ($r \leq 1$ Mpc) and time ($z = 1$ to $z = 0$).

The value $\rho/n$, by which we mean the average galaxy number density divided by the average density of the ICM, characterizes the enrichment behavior of the clusters, as will be made clear in the following section. The values for our model clusters are listed in Table 2. In our model clusters, the depth of the potential determines the density of the ICM. The cluster with the deepest potential (1) is also richest in galaxies, but it nevertheless has the highest $\rho/n$ value. This of course relies on assumptions made in the simulations, such as the baryon fraction or criteria for when galaxies form.

All our model clusters are "standard" clusters in the sense that they do not contain a cD galaxy or a cooling core.

## 4. Results

In the following subsection, we present the results of simulations performed with the standard parameter values chosen in Sect. 2.2. Thereafter, in Sect. 4.2, we discuss how a variation of these values affects the results.

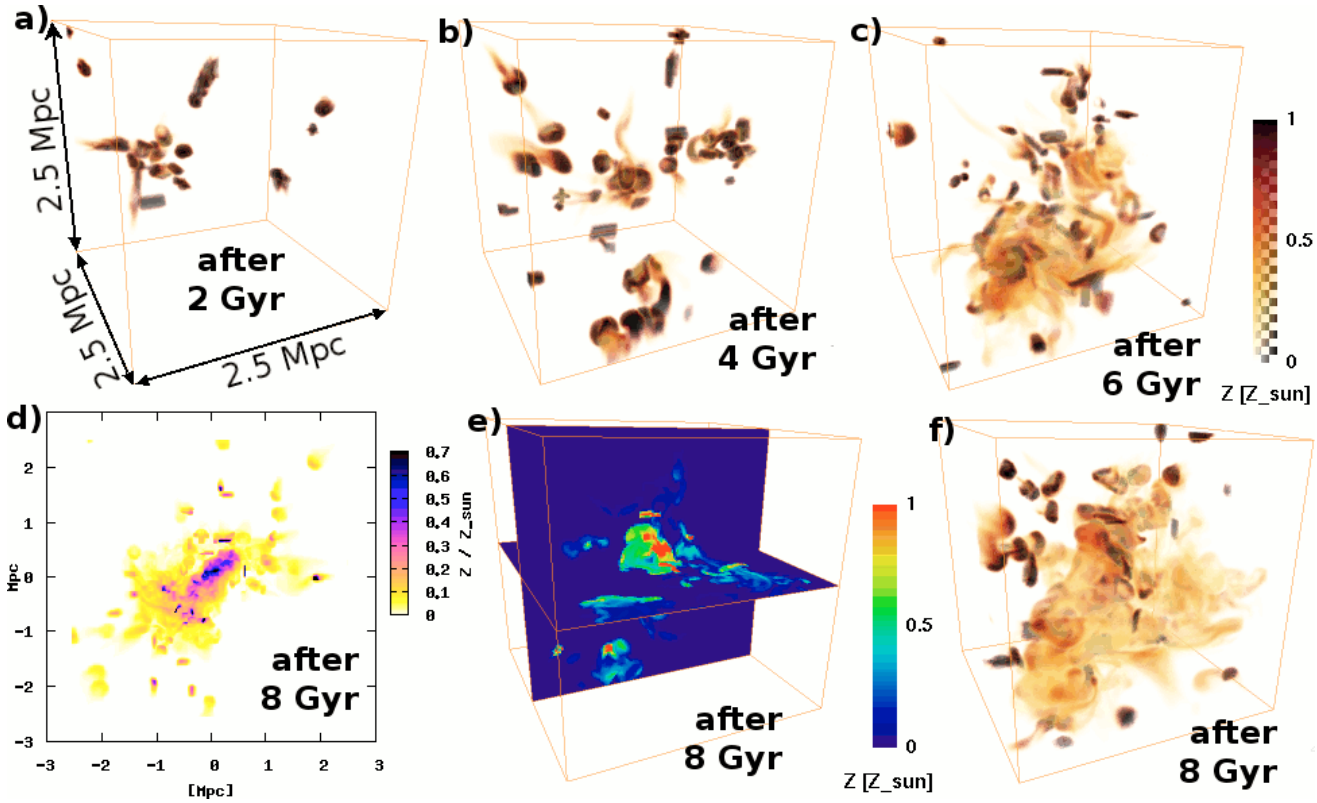


**Fig. 3.** Distribution of the metals in simulation 2b, **a)**, **b)**, **c)**, and **f)** show the evolution of the distribution in the innermost grid. The metals released into the ICM by the individual AGNs follow the merging process and get mixed quite thoroughly. Nevertheless, the final distribution is not homogeneous; **e)** depicts slices through the final distribution, revealing that most metals reside in the core region; **d)** shows what X-ray observations of the model cluster would ideally offer, if the model cluster was observed through an X-ray telescope with high resolution and high sensitivity.

**Table 3.** Parameter sets for the simulations presented in Sect. 4.1: (from left to right) fraction of galaxies with AGN outflows, duty cycle, outflow rate, outflow metallicity, outflow temperature, and energy outflow rate per AGN.

| | $f_{\rm AGN}$ | $\tau_{\rm AGN}$ [Gyr] | $\dot{M}_{\rm out}$ [$M_\odot$ yr$^{-1}$] | $Z_{\rm out}$ [$Z_\odot$] | $T_{\rm out}$ [K] | $\dot{E}_{\rm out}$ [J s$^{-1}$] |
|---|---|---|---|---|---|---|
| a | 0.05 | 0.1 | 0.5 | 5 | $10^6$ | $6.0 \times 10^{32}$ |
| b | 0.005 | 0.1 | 5 | 5 | $10^6$ | $6.0 \times 10^{33}$ |

a: Ejected material is distributed point-like; b: ejected material is distributed jet-like.

**Table 4.** Average metallicities within $r \leq 1$ Mpc from the 3d data and from the corresponding X-ray emission-weighted metallicity maps[a] at $z = 0$, mean number of AGNs and total mass of the metals directly released into the ICM in the mentioned region during the simulated time interval from $z = 1$ to $z = 0$.

| | $Z_{\rm 3d}$ [$Z_\odot$] | $Z_{\rm map}$ [$Z_\odot$] | mean # of AGNs | $Z_{\rm out} M_{\rm out,tot}$ [$10^9$ $M_\odot$] |
|---|---|---|---|---|
| 1a | 0.027 | 0.048 | 22.6 | 9.1 |
| 1b | 0.030 | 0.053 | 2.3 | 9.4 |
| 2a | 0.082 | 0.108 | 10.0 | 4.1 |
| 2b | 0.097 | 0.153 | 1.1 | 4.4 |
| 3a | 0.048 | 0.083 | 18.0 | 7.3 |
| 3b | 0.050 | 0.106 | 1.9 | 7.9 |

[a] Here, the average is weighted with surface brightness.

### 4.1. Metallicity distributions

The parameters for the simulations presented in this section are listed in Table 3. In the simulations (a) we assume that every AGN in the cluster has a moderate wind-like outflow, whereas in the simulations (b) we assume that radio-loud AGNs initiate massive outflows through entrainment by extended jets. The material is initially distributed in just one cell in the former case, and in several cells in the shape of bipolar jets in the latter. The specific values of the parameters are accounted for in Sect. 2.2. They have been tuned so that the total amount of metals released into the ICM is about equal in both cases, which facilitates a comparison. Forthwith, "2b" refers to model cluster 2 in simulation (b), etc.

Figure 3 illustrates how the metals are added to the ICM and how they are affected by the ICM dynamics in the case of the merging cluster 2 with jet-like outflows from radio-loud AGNs (b). At $z = 1$, the simulation starts with the ICM having $Z \equiv 0$. Metal-rich material from AGNs is inserted at various positions. It has the same velocity as the AGN host galaxy and is accelerated along with the rest of the ICM towards the center of the cube, where the merging occurs. The jet-like shape in which the material is initially distributed is quickly disrupted by this movement. In the end, we find a blurred, but inhomogeneous, region of high metallicity in the cluster center. The simulation clearly shows that much of the metal that ended up in the center were ejected at much larger radii.

The average metallicities in the cluster cores of the models in all simulations can be found in Table 4. The emission-weighted projection does not reveal the true metallicity but is approximately 60% higher. Although more than twice the amount

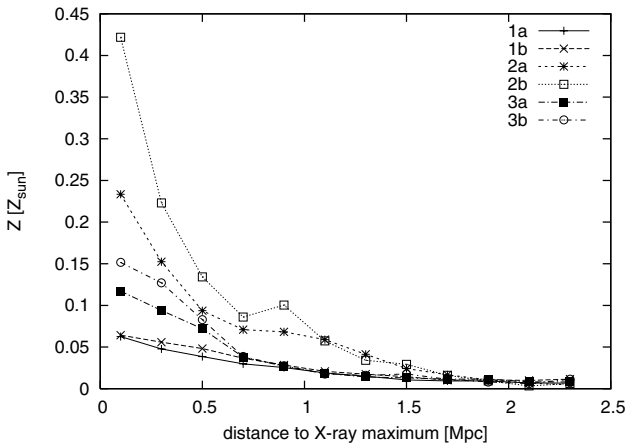


**Fig. 4.** Radial metallicity profiles, created from the metallicity maps at $z = 0$. The bin width is 0.2 Mpc and the values in the bins have been weighted with the X-ray surface brightness. The profiles are slightly different for the two simulations (a) and (b).

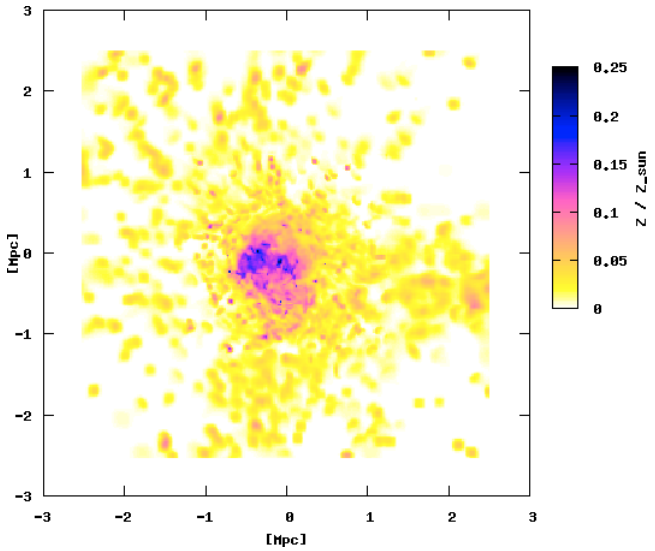


**Fig. 5.** X-ray emission-weighted metallicity map of model cluster 3 in simulation (a), where all AGNs are supposed to have wind-like outflows with 0.5 $M_\odot$ yr$^{-1}$, at $z = 0$. Figure 6 shows the same for simulation (b).

of metals are ejected in the case of cluster 1 (the rich cluster) compared to cluster 2 (the poor, merging cluster), the latter has a metallicity that is on average more than three times as high. Cluster 3 lies in between. This correlates well with the values of $\rho/n$ listed in Table 2. A cluster with a low $\rho/n$ gets enriched more than a cluster with a high $\rho/n$ and vice versa.

The radial profiles of the 2D metallicity, depicted in Fig. 4, show that most of the material ends up in the center of the clusters. Artificial X-ray emission-weighted metallicity maps of the standard cluster 3 in both simulation scenarios are depicted in Figs. 5 and 6. The parameter set (b) was chosen so as to compensate for a lower AGN fraction with a higher outflow rate. Nevertheless, the differences between (a) and (b) are quite dramatic, as a comparison of Figs. 5 and 6 shows. The map in Fig. 5 shows a pockmarked structure, whereas the map in Fig. 6 is dominated by single outflows that have not yet mixed with the surrounding material.

The initial distribution of the outflowing material (point-like or jet-like) turned out to be only of minor consequence to the

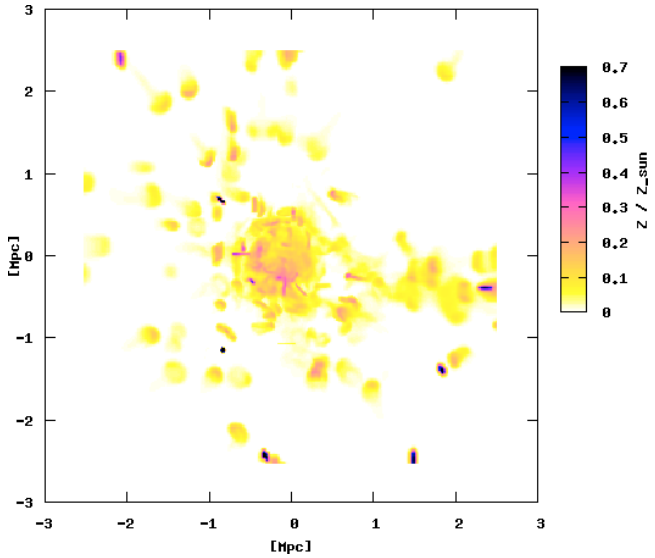


**Fig. 6.** X-ray emission-weighted metallicity map of model cluster 3 in simulation (b), where the radio-loud AGNs are supposed to eject metals into the ICM through entrainment by the jets, at $z = 0$. Although the total amount of metals is the same as in simulation (a), see Fig. 5, it shows a different structure with higher peak metallicities.

resulting metallicity distribution. The jet-like structures quickly ($\lesssim$1 Gyr) dissolve.

Considering that we only simulated about half of the time that was probably available for AGNs to enrich the ICM, and keeping in mind that AGNs might have been more numerous before $z = 1$, we see that both scenarios may explain the observed metal abundances in the ICM; e.g., Schmidt et al. (2002) find $Z = 0.3 \ldots 0.6$ in the core, $r \leq 125$ kpc, of the Perseus cluster. Also, in accordance with observations, the distribution is invariably inhomogeneous.

### 4.2. Parameter variations

Since the parameters describing the outflows and the outflow-capable AGN population of a cluster are not constrained very well, it is worthwile making a parameter study. Of course, we know that the population of AGNs is very inhomogeneous. The way we used the parameters here is only a crude approximation to get a first notion of how they affect the resulting metallicity. Unsurprisingly, the average metallicity in a region covering the main cluster is linearly dependent on $f_{\rm AGN}$, $\dot{M}_{\rm out}$, and $Z_{\rm out}$. The difference between a low $f_{\rm AGN}$ and a high one is obvious from Figs. 5 and 6.

Very massive outflows ($\gtrsim$5 $M_\odot$ for standard runs, especially in clusters with a low $\rho/n$ value and for the simulations (a), where the material was distributed into just one cell) can create features in the X-ray surface brightness and the temperature maps, where the ICM is both brighter and cooler than the surroundings. These features are caused by gas that is both cooler and denser than the surroundings, where material ejected by AGNs has not yet mixed thoroughly with the ambient medium. This is interesting because surface brightness maps from observations are available at much higher resolution and for larger regions than metallicity maps. If lots of AGNs have massive outflows like that (e.g. 5% of the total galaxy population), both the surface brightness and temperature maps from the simulations reveal a flaky structure that does not comply with observations. Therefore, we discarded such models.

The value of $Z_{\rm out}$ only affects the resulting metallicity values, not their distribution. This is to be understood as follows: a metallicity map resulting from a simulation where $Z_{\rm out} = x$ can be reproduced from a metallicity map from a similar simulation where $Z_{\rm out} = y$ by multiplying the latter with $x/y$. Given that $T_{\rm out}$ is the same, a different $Z_{\rm out}$ means a different $\dot{E}_{\rm out}$ (as the latter depends on the molecular weight), but the difference is minor. Thus, one can easily convert a map like that in Fig. 5 into one in which $Z_{\rm out}$ is different by simply multiplying the values on the colorbar with the respective factor.

Then, $\tau_{\rm AGN}$ determines how often the hosts of AGNs are changed. Thus, a shorter duty cycle means that the metal-rich gas from AGN outflows is dispersed more right from the start. This yields smoother metallicity maps.

Together with $\dot{M}_{\rm out}$ and $Z_{\rm out}$, $T_{\rm out}$ determines the energy outflow rate $\dot{E}_{\rm out}$. Putting a significant amount of energy into a cell of the model ICM results in vigorous convective movements, as a large portion of the energy is converted into kinetic energy. The resulting metallicity map is much smoother and has a lower peak. For the simulations presented in the preceding sections, this would happen if $T_{\rm out} \sim 10^9$ K. Below that, the value of the temperature is irrelevant to the final result.

## 5. Conclusions and outlook

We find that, when using a variety of assumptions based on observations, outflows from AGNs can contribute significantly to the metal content of the ICM or even explain its complete abundance. Furthermore, the resulting metallicity distribution resulting from the simulations is always inhomogeneous, in agreement with observations. We showed that the allowable range for the AGN outflow rate can be constrained by comparing the simulations with observations. General outflow rates $\gtrsim 5\ M_\odot\ {\rm yr}^{-1}$ yield unrealistic results if the material is initially distributed in a volume of $\lesssim (20\ {\rm kpc})^3$.

However, AGNs are currently not understood well enough to definitely estimate their importance concerning metal enrichment. Apart from a better understanding of AGNs, including triggering mechanisms and the origin of the apparent differences between them, the following questions need to be addressed: What is the exact outflow rate of AGN outflows leaving the galaxy? How are outflows initially distributed in the ICM? Is the outflow continuous? How significant is the role of AGN jets? And how does all this depend on the properties of the host galaxy? A self-consistent model of AGN outflows and jet simulations in a realistic, non-homogeneous environment would be helpful and will hopefully provide quantitative answers to some of these questions in the future.

The cluster simulations are currently being improved by the implementation of new initial conditions for the hydrodynamic simulations that will allow us to start them at a higher redshift. Preliminary tests have shown that this results in higher gas velocities, which leads to better intermixture between the material ejected by the galaxies and the ICM, especially in the outskirts of the model clusters. However, the inhomogeneity seems to be preserved. Future plans also include calculating many different elements separately instead of only distinguishing between hydrogen & helium and metals. However, most important of all is certainly a better understanding of AGN outflows.

*Acknowledgements.* This work was supported by the Austrian Science Foundation FWF (P15868, P18523, and P18416), by UniInfrastruktur 2005/2006, the DFG (Zi 663/6.1), AUSTRIAN GRID, by a University of Innsbruck scholarship, and by ESO Mobilitätsstipendien of the Austrian Ministry of Science. We thank Chiara Ferrari for interesting discussions.

## References

Baldwin, J. A., Hamann, F., Korista, K. T., et al. 2003, ApJ, 583, 649
Barnes, J., & Hut, P. 1986, Nature, 324, 446
Chartas, G., Brandt, W. N., & Gallagher, S. C. 2003, ApJ, 595, 85
Colella, P., & Woodward, P. R. 1984, J. Comp. Phys., 54, 174
Crenshaw, D. M., Kraemer, S. B., & George, I. M. 2003, ARA&A, 41, 117
Croton, D. J., Springel, V., White, S. D. M., et al. 2006, MNRAS, 365, 11
De Lucia, G., Kauffmann, G., & White, S. D. M. 2004, MNRAS, 349, 1101
De Young, D. S. 1978, ApJ, 223, 47
De Young, D. S. 1986, ApJ, 307, 62
Domainko, W., Gitti, M., Schindler, S., & Kapferer, W. 2004, A&A, 425, L21
Domainko, W., Mair, M., Kapferer, W., et al. 2006, A&A, 452, 795
Durret, F., Lima Neto, G. B., & Forman, W. 2005, A&A, 432, 809
Elvis, M. 2000, ApJ, 545, 63
Fryxell, B., Müller, E., & Arnett, D. 1989, MPA Report, 449
Gunn, J. E., & Gott, J. R. I. 1972, ApJ, 176, 1
Hamann, F. 1997, ApJS, 109, 279
Hamann, F. W., Barlow, T. A., Chaffee, F. C., Foltz, C. B., & Weymann, R. J. 2001, ApJ, 550, 142
Hasinger, G., Schartel, N., & Komossa, S. 2002, ApJ, 573, L77
Hayakawa, A., Furusho, T., Yamasaki, N. Y., Ishida, M., & Ohashi, T. 2004, PASJ, 56, 743
Hirotani, K. 2005, ApJ, 619, 73
Hoffman, Y., & Ribak, E. 1991, ApJ, 380, L5
Iwasawa, K., Fabian, A. C., Allen, S. W., & Ettori, S. 2001, MNRAS, 328, L5
Kapferer, W., Knapp, A., Schindler, S., Kimeswenger, S., & van Kampen, E. 2005, A&A, 438, 87
Kapferer, W., Ferrari, C., Domainko, W., et al. 2006, A&A, 447, 827
Krolik, J. H. 1999, Active galactic nuclei: from the central black hole to the galactic environment (Active galactic nuclei: from the central black hole to the galactic environment/Julian H. Krolik (Princeton, N. J.: Princeton University Press)
Martini, P. 2004, in Coevolution of Black Holes and Galaxies, ed. L. C. Ho (Cambridge: Cambridge Univ. Press), 170
Martini, P., Kelson, D. D., Kim, E., Mulchaey, J. S., & Athey, A. A. 2006, ApJ, 644, 116
Miller, N. A., & Owen, F. N. 2002, AJ, 124, 2453
Morganti, R., Tadhunter, C. N., & Oosterloo, T. A. 2005, A&A, 444, L9
Nagashima, M., Lacey, C. G., Baugh, C. M., Frenk, C. S., & Cole, S. 2005, MNRAS, 358, 1247
Owen, F. N., Odea, C. P., Inoue, M., & Eilek, J. A. 1985, ApJ, 294, L85
Ruffert, M. 1992, A&A, 265, 82
Sanders, J. S., Fabian, A. C., Allen, S. W., & Schmidt, R. W. 2004, MNRAS, 349, 952
Schindler, S., Kapferer, W., Domainko, W., et al. 2005, A&A, 435, L25
Schmidt, R. W., Fabian, A. C., & Sanders, J. S. 2002, MNRAS, 337, 71
Sijacki, D., & Springel, V. 2006, MNRAS, 366, 397
Tamura, T., Kaastra, J. S., den Herder, J. W. A., Bleeker, J. A. M., & Peterson, J. R. 2004, A&A, 420, 135
Tornatore, L., Borgani, S., Matteucci, F., Recchi, S., & Tozzi, P. 2004, MNRAS, 349, L19
van de Weygaert, R., & Bertschinger, E. 1996, MNRAS, 281, 84
van Kampen, E., Jimenez, R., & Peacock, J. A. 1999, MNRAS, 310, 43
Veilleux, S., Cecil, G., & Bland-Hawthorn, J. 2005, ARA&A, 43, 769
Vikhlinin, A., Markevitch, M., Murray, S. S., et al. 2005, ApJ, 628, 655